An adaptive descriptor for uncalibrated omnidirectional images - towards scene reconstruction by trifocal tensor

Ming Liu, Bekir Tufan Alper, Roland Siegwart
Autonomous Systems Lab, ETH Zurich, Switzerland
ming.liu@mavt.ethz.ch, btalper@sabanciuniv.edu, rsiegwart@ethz.ch

***Abstract*—Omnidirectional cameras are widely used for robotic applications in structured environments. However, because of the distorted field of view (FOV), it is hard to describe the primitive features extracted from them robustly. In this paper, we tackle the problem by using Histogram of Gradient (HoG) statistics for the regions of interest (ROI) in the neighborhood of major vertical lines extracted from the panoramic image. As a validation, we compare the proposed algorithm with state-of-the-art based on two widely used data-sets, leading to evidently better performance. We also introduce a scene reconstruction scenario using the proposed descriptor based on 1D Trifocal Tensor framework. The comparative results show the competence of the descriptor.**

I. Introduction

A. Motivation

Scene representation is a subtle problem, especially when non-standard imaging sensors such as omnidirectional camera is used. Although the representations based on calibration is less a problem nowadays [1], algorithms that independent from calibration result are still preferred, due to complexity and generalization potentials.

Omnidirectional camera is considered to be one of the most efficient sensors for environment modeling [2], [3]. However, a reliable descriptor for the conducted panoramic images is still required to be developed and properly evaluated. Considering the characteristics of omnidirectional cameras, the most reliable feature is the vertical lines perpendicular to the motion plane, which are preserved regardless rotation and translation.

In this paper, we propose an adaptive descriptor for major vertical lines, which is inspired by and extended from [4]. We evaluate the performance in two steps. First we evaluate matching precision against [4] using two widely used data-sets. Besides, we present a scene reconstruction scenario using trifocal tensor [5], as an application of the proposed feature.

B. Related Work

Several techniques are used to describe the surrounding environment of a robot. One of the major differences lies in the various descriptors used by structure reconstruction. We see that many algorithms utilize key-point based features on perspective cameras, e.g. PTAM [6] uses mainly FAST corners[7]; FAB-MAP [8] uses mainly SIFT [9] or SURF [10]. However, not many applications or descriptors have been reported on omnidirectional camera, such as the example depicted in figure 1. The main reason is the distortion introduced by the nonlinear transformation from the mirror shape, by which the nonuniform resolution will greatly affect the stability of patch based descriptors.

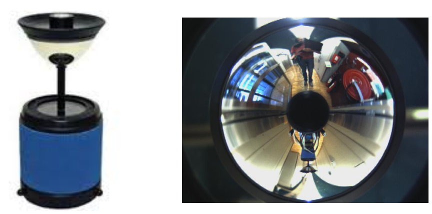

Fig. 1. Omnidirectional camera and panoramic image

There are two ways to represent the environment by images: First, descriptors are extracted from the whole image, e.g. by Fourier transformation [11], [12], [13]. Among the existing algorithms designed for omnidirectional camera, "Fingerprint of places" [14] and FACT [15], [3] are color based features, where the vertical line is considered as an important hint for the formation of descriptors of the whole image. The second category is object oriented representations [16], [17], [18] namely feature based algorithms. Several lightweight key-point descriptors were developed [19], [20] and got widely applied in scene recognition problems [21], [22].

We notice that beside the wide FOV, an important reason for choosing omnidirectional vision is that, when the camera is mounted perpendicularly to the plane of motion, the vertical lines of the scene are mapped into radial lines on the images. Regarding the descriptor for the vertical lines, [4] defines a line descriptor using HoG extracted from static circular patterns. However, we find it is hard to adapt it to robot translation, by which the length of critical vertical lines varies, due to the ROI is fixed even for completely different image frames. In this paper, we propose that the ROI need to adapt to different environments. The parameter selection are evaluated accordingly.

There are two groups of techniques to work on vertical line matching. The first group deals with the individual line segments such as [23], [4] and the second one works with the union of the line segments [24], [25], [26]. Considering the complexity of the second group, in this paper we use the separation angle between two descriptor vectors as the primary metric to represent the similarity.

This work was supported by the EU FP7 project NIFTi (contract # 247870).

The panoramic images taken from omnidirectional camera are used with the raw image or an unwrapped representation. In the case of full calibration, the raw image is usually projected to spheres [1]. However, when we only focus on the vertical lines, the unwrapping along the horizontal line is more feasible [27], [28], [29]. This unwrapping process only depends on a calibration of the image center and extraction of the main circular shape as the right image in figure 1, which can be easily dealt with by Hough transformation.

In order to reconstruct scene appearances, the feature positions are recovered by geometrical constraints. In this paper, we use 1D Trifocal Tensor [30] to realize this computation process, which is mostly used in visual homing problem [30]. Comparing with other homing algorithms [31], [32], the trifocal tensor results in not only robot positions, but also feature distributions. This provides a basis for scene reconstruction. We use the proposed features to provide a group of geometrical constraints in this work.

C. Organisation

The rest of this paper is organized as follows. We first introduce the feature extraction and description in section II. Then, the scene reconstruction algorithm is outlined in section III. The parametrization and evaluation will be carried out with widely cited data-sets in section IV, followed by conclusion of this work in the end.

II. Proposed Descriptor

In this section, we introduce the major processes to detect salient features, namely vertical lines, and the descriptor formation.

A. Feature Detection

An unwrapped image facilitates the extraction of major vertical lines, since all the radial lines are projected into vertical direction. Hough Circle Detection algorithm is first performed in order to obtain the radius of effective FOV and the center coordinate. The detection results is shown as figure 2. The outermost circle is taken as the effective FOV, since its inner part covers all valid information of the panoramic image. The estimated image center is taken by the circle center shown in figure 2(c).

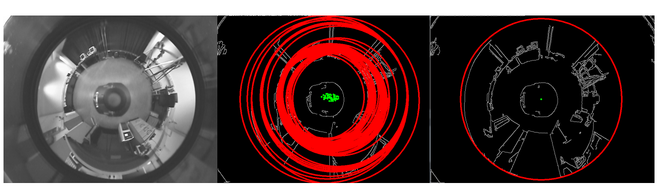

(a) Raw Image (b) Detected circles (c) Outer circle

Fig. 2. All the circles detected in the raw image. The outermost circle is extracted.

Major vertical lines are then extracted following the similar algorithm as shown in [15].

B. Descriptor Formulation

In order to match the vertical lines across images, the formation of the descriptor is essential. Sometimes a tracking scheme is adopted to help the matching process, where detected features have to be matched between two consecutive images [4]. In this work, we emphasize the appearance based matching without considering the tracking results.

We build the descriptor using the Histogram of Oriented Gradient (HoG). Considering the limitation of fixed circular shapes used by [4], we reshape the ROI by rectangles. For each major vertical line, a set of 6 ROI rectangles is extracted as shown in figure 3, where the width of rectangle is adapted for different environments.

Fig. 3. The shape of the modified descriptor with varying $scaleX$. The width of the descriptor is changed to adapt different environments.

In order to calculate the HoG efficiently, the orientation space is divided ranged from $-\pi$ to π into N_b bins. Then two components of the image gradients for x- and y-directions, I_x and I_y, are calculated for each pixel in each rectangle. The frequencies per phase are clustered, according to the discretized phase of the gradients Φ.

$$M = \sqrt{I_x^2 + I_y^2}, \;\; \Phi = \arctan(I_y, I_x) \tag{1}$$

Afterward, the gradient magnitude M of each pixel is accumulated in the corresponding bin over the Φ space. An example of the calculated HoG is shown in figure 4.

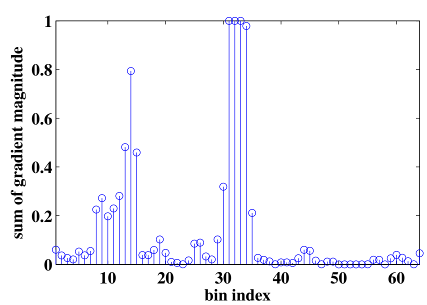

Fig. 4. An instance of non-normalized HoG with N_b = 32 bins.

The accumulated magnitude values are normalized in each rectangle as the value with the maximum gradient magnitude is equal to one. All the bins with magnitude value greater than 0.1 (10% of the maximum value) are threshold as 0.1, then perform normalization again. This extra operation makes the descriptor more robust changes since the gradient magnitudes are more sensitive than orientation, in the case of illumination changes. At the end, three pairs of histograms H_1, H_2 and H_3 regarding left and right side of a vertical line are used as descriptor:

$$\begin{array}{l} H_1 = [H_{1,L}, H_{1,R}] \\ H_2 = [H_{2,L}, H_{2,R}] \\ H_3 = [H_{3,L}, H_{3,R}] \end{array} \tag{2}$$

We see that two major parameters determine the descriptor for a given image, i.e. number of bins for the HoG N_b and width of the rectangle, indicated by $scaleX$. For different specific environment, the optimal parameter set varies. The parametrization is evaluated in section IV.

C. Feature matching

In order to measure the similarity between two descriptors, we consider a descriptor as a vector with $6 \times N_b$ dimensions. Intuitively, we take the separate angle of two normalized descriptors $\mathbf{x}, \mathbf{y}$ as the measure of the distance, as:

$$\alpha(x, y) = \frac{\langle \mathbf{x}, \mathbf{y} \rangle}{|\mathbf{x}||\mathbf{y}|} \tag{3}$$

where $\langle \mathbf{x}, \mathbf{y} \rangle$ denotes the inner product of the two descriptors. When comparing the features from two images A and B, letting $[A_1, A_2, .., A_m]$ be the descriptors of image A and $[B_1, B_2, .., B_n]$ be the descriptors of B, a positive matching is validated by the second best match is smaller than r_{th} ratio of the best match. Specifically, a scoring method has been implemented, following the definitions as follows. $maxIP$ is the maximum of inner product result, triggered by a pair of best matches, which is the closest to 1, $SmaxIP$ is the second maximum, and $avgIP$ is the average of all possible descriptor pairs of A_i and B_j, with $j = 1, 2, ..n$. The final score is achieved by comparing the $maxIP$ with $SmaxIP$ and $avgIP$ of all the descriptors in the second image, as follows.

$$\begin{cases} \text{Condition:} score1 \times score2 \times maxIP > r_{th} \\ score1 = \dfrac{maxIP}{SmaxIP} \\ score2 = \dfrac{maxIP}{avgIP} \end{cases} \tag{4}$$

where we use an empirical $r_{th} = 80\%$.

Considering the operation on a sequence of images, especially for tracking problems, we use a naive strategy as follows. After matching the lines in the first two images, the same procedure is applied for the second and the third images for the vertical lines that have already been matched previously. As a sample result, a group of matched triple in three consecutive images is illustrated as in figure 5.

III. Scene Reconstruction

Using trifocal tensor for scene reconstruction, the system needs bearing angles of matched features from three different robot positions. By using these three view bearing information, the 1D trifocal tensor is calculated [30]. The trifocal tensor gives a constraint on relative position and orientation of three different robot positions. Given the estimated relative positions, by triangulating the landmarks, the geometrical structural information can be recovered.

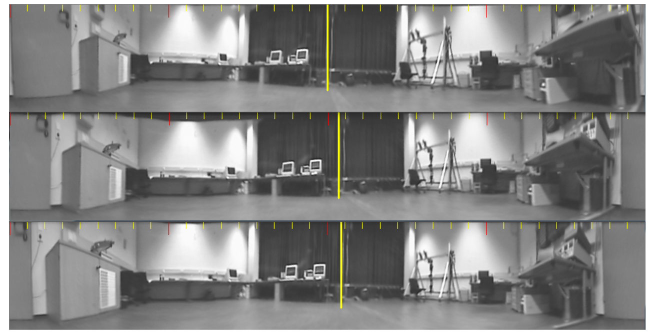

Fig. 5. An example of matched vertical line triples. The bearing information calculated for each image is used for trifocal tensor calculation.

A. Tensor Calculation

For the tensor calculation, we use the 1D trifocal tensor introduced in [33], [34] as basis. We concisely outline the process as follows.

The inputs of the tensor calculation process is at least seven bearing information triple that comes from three different robot positions. The bearing information from each major vertical line is kept in a state vector $u = (\sin\alpha, \cos\alpha)^T$, where α is the bearing angle of a line feature.

Following the notation of [33], θ's are used to present the robot heading and t_x, t_y are used to denote the translation in x- and y-direction for each local frame. The trifocal tensor is represented as:

$$\mathbf{T} = [T_{111}\ T_{112}\ T_{121}\ T_{122}\ T_{211}\ T_{212}\ T_{221}\ T_{222}]^T$$

where

$$\begin{array}{l} T_{111} = t_y^{'} sin(\theta^{''}) - t_y^{''} sin(\theta^{'}); \\ T_{112} = t_y^{'} cos(\theta^{''}) + t_x^{''} sin(\theta^{'}); \\ T_{121} = -t_x^{'} sin(\theta^{''}) - t_y^{''} cos(\theta^{'}); \\ T_{122} = -t_x^{'} cos(\theta^{''}) + t_x^{''} cos(\theta^{'}); \\ T_{211} = -t_y^{'} cos(\theta^{''}) + t_y^{''} cos(\theta^{'}); \\ T_{212} = t_y^{'} sin(\theta^{''}) - t_x^{''} cos(\theta^{'}); \\ T_{221} = t_x^{'} cos(\theta^{''}) - t_y^{''} sin(\theta^{'}); \\ T_{222} = -t_x^{'} sin(\theta^{''}) + t_x^{''} sin(\theta^{'}). \end{array} \tag{5}$$

The trifocal constraints is composed by the coefficient matrix A and tensor $\mathbf{T}$ as (5).

$$\begin{aligned} A\mathbf{T} = & [u_1 u_1^{'} u_1^{''}\ u_1 u_1^{'} u_2^{''}\ u_1 u_2^{'} u_1^{''}\ u_1 u_2^{'} u_2^{''} \\ & u_2 u_1^{'} u_1^{''}\ u_2 u_1^{'} u_2^{''}\ u_2 u_2^{'} u_1^{''}\ u_2 u_2^{'} u_2^{''}]\mathbf{T} = 0 \end{aligned} \tag{6}$$

In order to solve approximated trifocal tensor T, the eigenvector associated with the smallest eigenvalue of the matrix $A^T A$ is used, which theoretically obtained by singular value decomposition (SVD) of matrix A.

IV. Evaluation & Validation

A. Overview and Data-set

Two open source online data-sets are adopted to validate the proposed descriptors. Both data-sets are built with a mirrored omni-directional camera mounted on mobile wheeled robots for indoor environments [35], [36].

For each sample of a database, the feature matching is evaluated and compared with the state-of-art descriptor [4], in terms of true positive ratio. Please notice that the algorithm complexity for [4] and the proposed method is similar, since they both use HoG description. Therefore, the execution time is not taken for comparison.

B. Parameter Selection

In order to optimize the parameters, for specific environments the two major parameters are to be selected based on sample statistics. The ranges of parameters are: N_b values are varied from 16 to 72, with increments by 4; the width of the descriptor($scaleX$) varies from 0.1 to 0.8, with increments by 0.1. We construct comparison matrices based on the true positive rates of the two descriptors on random samples. The results for the two data-sets are shown in table I, II and table III, IV, respectively.

We have the following observations for this part of evaluation:

- The proposed algorithm performs better in both data-sets.
- The increment of number of bins for HoG helps the matching. However this correction will have less effect when it reached to a certain large number. Considering the complexity of the histogram construction and feature matching is related to N_b, a sufficient selection is the knee value in the plot by table I to IV.
- For both descriptors, the performance is worse for the COLD data-set. We observe the major reason is that the frame-edges of glass doors and windows in the COLD data-set triggers frequently wrong description by considering the scene behind. For the case of Vardy data-set, the appearances of the major vertical lines are usually not affected by perspective changes. This is the limitation for both descriptors.

As a result, the parameter set $\{N_b, scaleX\}$ for COLD data-set is $\{52, 0.6\}$, and $\{36, 0.4\}$ for Varday data-set. We see that the introduced adaptive parameter $scaleX$ greatly optimize the performance of the descriptor.

C. Reconstruction

We evaluate the performance for scene reconstruction by trifocal tensor. A typical failure case is shown in figure 7(b) and (c). The reconstructed robot positions are good enough for robot homing problems, however, the reconstruction of landmark distribution is poorly obtained. We found it is related to two characteristics of the coefficient matrix A, the smallest eigenvalue $(\min \lambda_i)$ and the condition number of the matrix A $(cond(A))$. $\min \lambda_i$ defines the precision of trifocal tensor estimation by SVD, and $cond(A)$ reflect the stability of the solution to equation 5. These two criteria are taken as further assessment of the reconstruction quality.

1) Effect on the smallest eigenvalue: By increasing the standard deviation of the observation noise from 0.1 to 10, we show the uncertainty of the simulated features in figure 6, whereas $\min \lambda_i$ rises as depicted in figure 7. It implies that in order to have a reliable reconstruction, $\min \lambda_i$ needs to be as small as possible. Over a given threshold, the reconstruction results need to be discarded.

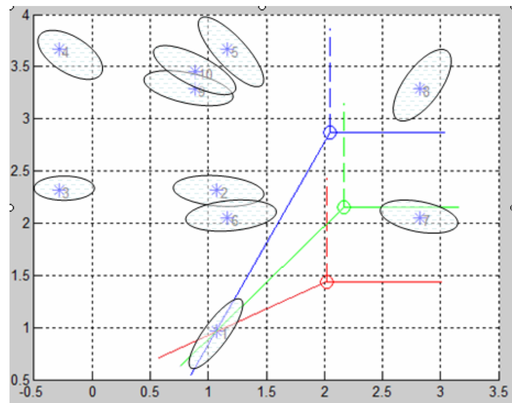

Fig. 6. Landmark locations with uncertainty.

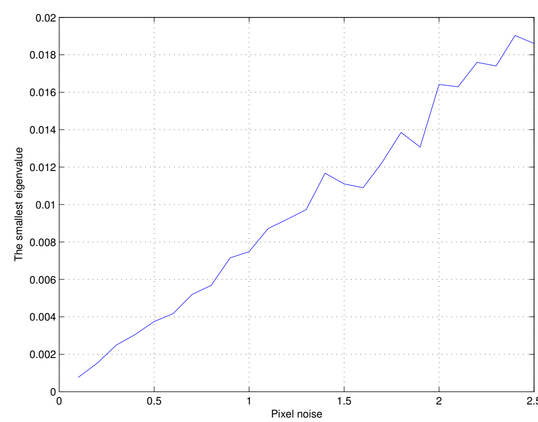

Fig. 7. Pixel noise vs The smallest eigenvalue.

2) Effect on the conditional number: For the second characteristic $cond(A)$, the relation to the variety in the bearing information is investigated. A larger conditional number generally leads to unreliable solutions for linear systems. In order to test how the perspective differences affect the robustness of reconstruction, we use different distances among the observing poses, depicted in figure 8. Intuitively, we can imagine that the closer the robot positions are, the more confused for the scene recognition. Figure 9 validates this assumption by plotting the relation between $cond(A)$ and the mean distance between two observation poses. We observe that a larger distance will optimize the quality of the reconstruction, but it usually leads to less positive matches for real data. Therefore compromise

$scaleX/N_b$	**16**	**20**	**24**	**28**	**32**	**36**	**40**	**44**	**48**	**52**	**56**	**60**	**64**	**68**	**72**
0.1	54.5	54.5	51.5	54.5	57.5	57.5	60.6	60.6	60.6	60.6	60.6	60.6	60.6	60.6	60.6
0.2	54.5	54.5	54.5	57.5	57.5	57.5	57.5	57.5	57.5	57.5	60.6	60.6	60.6	57.5	57.5
0.3	57.5	60.6	60.6	60.6	60.6	60.6	60.6	69.6	69.6	60.6	60.6	60.6	60.6	60.6	60.6
0.4	54.5	57.5	57.5	60.6	57.5	63.6	63.6	66.6	60.6	60.6	57.5	60.6	60.6	57.5	57.5
0.5	54.5	54.5	63.6	63.6	63.6	63.6	63.6	66.6	66.6	66.6	66.6	66.6	63.6	63.6	63.6
0.6	57.5	54.5	54.5	60.6	66.6	66.6	69.6	69.6	69.6	72.7	72.7	72.7	72.7	72.7	72.7
0.7	63.6	57.5	69.6	69.6	69.6	69.6	69.6	69.6	66.6	66.6	63.6	63.6	63.6	63.6	63.6
0.8	57.5	57.5	63.6	60.6	60.6	60.6	60.6	60.6	60.6	60.6	57.5	63.6	63.6	63.6	63.6

TABLE I
THE TRUE POSITIVE RATIO WITH THE PROPOSED DESCRIPTOR, BY VARYING N_b AND $scaleX$ (THE COLD DATA-SET).

N_b	**16**	**20**	**24**	**28**	**32**	**36**	**40**	**44**	**48**	**52**	**56**	**60**	**64**	**68**	**72**
	60.6	60.6	60.6	57.5	57.5	60.6	57.5	54.5	54.5	54.5	54.5	54.5	54.5	54.5	54.5

TABLE II
THE TRUE POSITIVE RATIO WITH [4], BY VARYING N_b (THE COLD DATA-SET).

$scaleX/N_b$	**16**	**20**	**24**	**28**	**32**	**36**	**40**	**44**	**48**	**52**	**56**	**60**	**64**	**68**	**72**
0.1	75.7	75.7	75.7	75.7	81.8	81.8	81.8	81.8	81.8	81.8	81.8	81.8	78.7	78.7	81.8
0.2	90.9	87.8	90.9	87.8	87.8	93.9	93.9	93.9	93.9	93.9	93.9	93.9	93.9	90.9	90.9
0.3	87.8	87.8	87.8	87.8	87.8	90.9	84.8	84.8	84.8	84.8	84.8	84.8	84.8	90.9	84.8
0.4	84.8	81.8	81.8	87.8	87.8	90.9	90.9	90.9	90.9	90.9	90.9	90.9	90.9	90.9	90.9
0.5	81.8	81.8	81.8	81.8	84.8	84.8	84.8	84.8	84.8	84.8	84.8	84.8	84.8	84.8	84.8
0.6	78.7	75.7	81.8	78.7	87.8	87.8	87.8	90.9	84.8	84.8	84.8	84.8	84.8	81.8	81.8
0.7	81.8	84.8	84.8	84.8	81.8	81.8	81.8	81.8	81.8	81.8	78.7	78.7	78.7	72.7	72.7
0.8	84.8	84.8	87.8	87.8	87.8	87.8	84.8	84.8	84.8	84.8	81.8	81.8	81.8	78.7	78.7

TABLE III
THE TRUE POSITIVE RATIO WITH THE PROPOSED DESCRIPTOR, BY VARYING N_b AND $scaleX$ (THE VARDY A1ORIGINALH DATA-SET)

N_b	**16**	**20**	**24**	**28**	**32**	**36**	**40**	**44**	**48**	**52**	**56**	**60**	**64**	**68**	**72**
	60.6	60.6	60.6	66.6	66.6	69.6	69.6	69.6	69.6	69.6	69.6	69.6	69.6	69.6	69.6

TABLE IV
THE TRUE POSITIVE RATIO WITH [4], BY VARYING N_b (THE VARDY A1ORIGINALH DATA-SET).

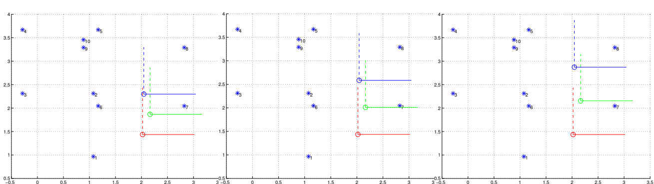

Fig. 8. Examples of various distances among robot positions. The effect of the distance variance is investigated while keeping the same feature distribution.

is required for threshold selection. [1]

3) Reconstruction result: Given the analysis on parametrization and quality justification, the scene reconstruction is carried out by firstly thresholding the aforementioned criteria. Unreliable matched feature sets are discarded. Then, geometrical information is calculated from equation (4) and (5) using Stimulated Annealing, using a single-shot odometry measure to correct the transformation scale between image space and real world. A qualitative result is shown in figure 10 using the images in figure 5.

[1] In this work, threshold for $\min \lambda_i$ is 0.02, and threshold for $cond(A)$ is 100.

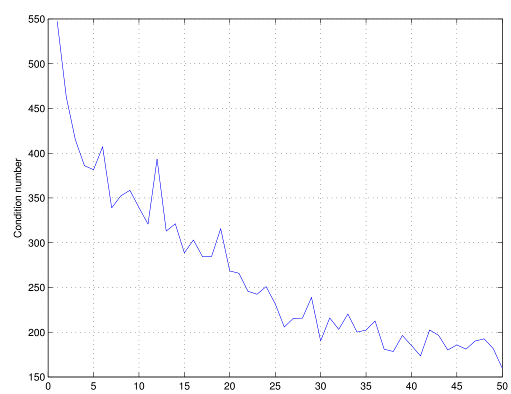

Fig. 9. Distance vs Condition number.

V. CONCLUSION

In this paper, we first introduced an adaptive descriptor designed for omnidirectional camera. It works on the panoramic images, independent of intrinsic calibration. It outperforms the state-of-the-art, in terms of recall precision as well. The proposed descriptor is validated by a scene reconstruction scenario. Beside, two criteria for scene recognition problem

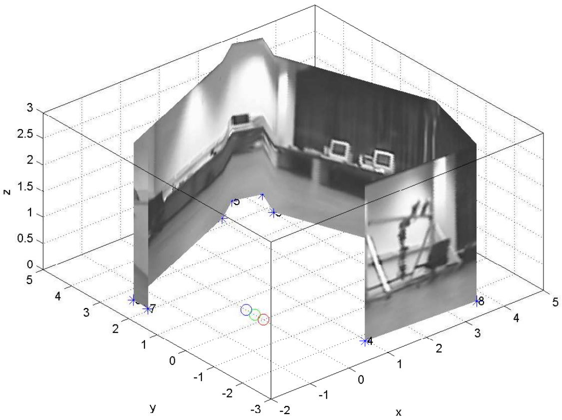

Fig. 10. Reconstructed environment in 3D by trifocal tensor

are proposed and validated through simulation. As future work, we will focus on applications using the proposed descriptor and quantitative assessment of the reconstruction quality.

References

[1] J. Cruz-Mota, I. Bogdanova, B. Paquier, M. Bierlaire, and J. Thiran, "Scale invariant feature transform on the sphere: Theory and applications," *International journal of computer vision*, pp. 1–25, 2012.

[2] N. Winters, J. Gaspar, G. Lacey, and J. Santos-Victor, "Omni-directional vision for robot navigation," in *Proceedings of the IEEE Workshop on Omnidirectional Vision*. IEEE, 2000, pp. 21–28.

[3] M. Liu and R. Siegwart, "DP-FACT: Towards topological mapping and scene recognition with color for omnidirectional camera," in *Proceedings of the IEEE International Conference on Robotics and Automation (ICRA)*, 2012.

[4] D. Scaramuzza, A. Martinelli, and R. Siegwart, "A robust descriptor for tracking vertical lines in omnidirectional images and its use in mobile robotics," *International Journal of Robotics Research*, 2009, special Issue on Field and Service Robotics.

[5] H. Becerra, G. López-Nicolas, and C. Sagüés, "Omnidirectional visual control of mobile robots based on the 1d trifocal tensor," *Robotics and Autonomous Systems*, vol. 58, no. 6, pp. 796–808, 2010.

[6] G. Klein and D. Murray, "Parallel tracking and mapping for small AR workspaces," in *Proc. Sixth IEEE and ACM International Symposium on Mixed and Augmented Reality (ISMAR)*, Nara, Japan, November 2007.

[7] M. Trajković and M. Hedley, "Fast corner detection," *Image and Vision Computing*, vol. 16, no. 2, pp. 75–87, 1998.

[8] M. Cummins and P. Newman, "Fab-map: Probabilistic localization and mapping in the space of appearance," *The International Journal of Robotics Research*, vol. 27, no. 6, pp. 647–665, 2008.

[9] D. Lowe, "Distinctive image features from scale-invariant keypoints," *International Journal of Computer Vision*, vol. 60, no. 2, pp. 91–110, 2004.

[10] H. Bay, T. Tuytelaars, and L. Van Gool, "SURF: Speeded up robust features," *Lecture notes in computer science*, vol. 3951, p. 404, 2006.

[11] X. Meng, Z. Wang, and L. Wu, "Building global image features for scene recognition," *Pattern Recognition*, 2011.

[12] A. Pretto, E. Menegatti, Y. Jitsukawa, R. Ueda, and T. Arai, "Image similarity based on discrete wavelet transform for robots with low-computational resources," *Robotics and Autonomous Systems*, vol. 58, no. 7, pp. 879–888, 2010.

[13] L. Payá, L. Fernández, A. Gil, and O. Reinoso, "Map building and monte carlo localization using global appearance of omnidirectional images," *Sensors*, vol. 10, no. 12, pp. 11 468–11 497, 2010.

[14] P. Lamon, A. Tapus, E. Glauser, N. Tomatis, and R. Siegwart, "Environmental modeling with fingerprint sequences for topological global localization," in *Proceedings of the IEEE/RSJ International Conference on Intelligent Robots and Systems (IROS)*, vol. 4, 2003.

[15] M. Liu, D. Scaramuzza, C. Pradalier, R. Siegwart, and Q. Chen, "Scene recognition with omnidirectional vision for topological map using lightweight adaptive descriptors," in *Proceedings of the IEEE/RSJ International Conference on Intelligent Robots and Systems (IROS)*. IEEE, 2009, pp. 116–121.

[16] A. Bosch, A. Zisserman, and X. Munoz, "Scene classification via plsa," *European Conference on Computer Vision (ECCV)*, pp. 517–530, 2006.

[17] A. Torralba, K. Murphy, W. Freeman, and M. Rubin, "Context-based vision system for place and object recognition," *Proceedings of the IEEE International Conference on Computer Vision (ICCV)*, 2003.

[18] S. Vasudevan, S. Gachter, V. Nguyen, and R. Siegwart, "Cognitive maps for mobile robots–an object based approach," *Robotics and Autonomous Systems*, vol. 55, no. 5, pp. 359 – 371, 2007, from Sensors to Human Spatial Concepts. [Online]. Available: http://www.sciencedirect.com/science/article/B6V16-4MY0MK7-1/2/e379fd59a33b6d0a42355ba120c444e9

[19] J. Wu and J. Rehg, "Centrist: A visual descriptor for scene categorization," *IEEE Transactions on Pattern Analysis and Machine Intelligence*, pp. 1489–1501, 2010.

[20] M. Calonder, V. Lepetit, and P. Fua, "Keypoint signatures for fast learning and recognition," *European Conference on Computer Vision (ECCV)*, pp. 58–71, 2008.

[21] J. Wu, H. Christensen, and J. Rehg, "Visual place categorization: problem, dataset, and algorithm," in *Proceedings of the IEEE/RSJ International Conference on Intelligent Robots and Systems (IROS)*. IEEE, 2009, pp. 4763–4770.

[22] A. Ranganathan, "PLISS: Detecting and Labeling Places Using Online Change-Point Detection," *Proceedings of Robotics: Science and Systems, Zaragoza, Spain*, 2010.

[23] Z. Zhang, "Token tracking in a cluttered scene," *Image and Vision Computing*, vol. 12, no. 2, pp. 110–120, 1994.

[24] J. Crowley, P. Stelmaszyk, T. Skordas, and P. Puget, "Measurement and integration of 3-d structures by tracking edge lines," *International Journal of Computer Vision*, vol. 8, no. 1, pp. 29–52, 1992.

[25] D. Huttenlocher, G. Klanderman, and W. Rucklidge, "Comparing images using the hausdorff distance," *Pattern Analysis and Machine Intelligence, IEEE Transactions on*, vol. 15, no. 9, pp. 850–863, 1993.

[26] R. Deriche and O. Faugeras, "Tracking line segments," *Image and Vision Computing*, vol. 8, no. 4, pp. 261–270, 1990.

[27] S. Nayar, "Catadioptric omnidirectional camera," in *Computer Vision and Pattern Recognition, 1997. Proceedings., 1997 IEEE Computer Society Conference on*. IEEE, 1997, pp. 482–488.

[28] T. Mauthner, F. Fraundorfer, and H. Bischof, "Region matching for omnidirectional images using virtual camera planes," in *Proc. of Computer Vision Winter Workshop*, 2006.

[29] M. Liu, C. Pradalier, F. Pomerleau, and R. Siegwart, "Scale-only Visual Homing from an Omnidirectional Camera," in *Proceedings of the IEEE International Conference on Robotics and Automation (ICRA)*, 2012.

[30] M. Aranda, G. Lopez-Nicolas, and C. Sagues, "Omnidirectional visual homing using the 1D trifocal tensor," in *Proceedings of the IEEE International Conference on Robotics and Automation (ICRA)*, 2010, pp. 2444–2450.

[31] M. Liu, C. Pradalier, F. Pomerleau, and R. Siegwart, "The role of homing in visual topological navigation," in *Proceedings of the IEEE/RSJ International Conference on Intelligent Robots and Systems (IROS)*, 2012.

[32] M. Liu, C. Pradalier, Q. Chen, and R. Siegwart, "A bearing-only 2D / 3D-homing method under a visual servoing framework," in *Proceedings of the IEEE International Conference on Robotics and Automation (ICRA)*, Anchorage Convention District, 2010, pp. 4062–4067.

[33] J. Guerrero, A. Murillo, and C. Sagues, "Localization and matching using the planar trifocal tensor with bearing-only data," *Robotics, IEEE Transactions on*, vol. 24, no. 2, pp. 494–501, 2008.

[34] O. Faugeras, L. Quan, and P. Sturm, "Self-calibration of a 1d projective camera and its application to the self-calibration of a 2d projective camera," *European Conference on Computer Vision (ECCV)*, pp. 36–52, 1998.

[35] A. Vardy, "Panoramic image database." [Online]. Available: http://www.ti.uni-bielefeld.de/html/research/avardy/index.html

[36] A. Pronobis and B. Caputo, "COLD: The CoSy localization database," *The International Journal of Robotics Research*, vol. 28, no. 5, pp. 588–594, 2009.